Journal of the Korean Society
for Nondestructive Testing
Vol. 23, No. 6 (2003. 12)

Transferring Distance-Amplitude Correction Curves - A Model-based Approach

Hak-Joon Kim*,†, Lester W. Schmerr Jr.*,**, Sung-Jin Song*** and Alexander Sedov****

Abstract In practice, it is common to manufacture reference blocks containing simple reflectors to obtain distance-amplitude correction (DAC) curves. However, the construction of DAC curves in this manner requires the use of a large number of specimens with appropriate curvatures and reference reflectors located at various depths. Therefore, less costly and quantitative procedures are strongly needed. To address such a need, in this study, we have developed model-based transfer curves to relate a DAC curve obtained in a particular reference configuration with that for a completely different configuration. An example of transferring DAC curves, using the proposed transfer curves, is given.

Keywords: DAC Curves, Ultrasonic Modeling, Transfer Curves, Reference Scatterer

1. Introduction

In ultrasonic standards practice, it is common to manufacture reference blocks containing simple reflectors, such as flat-bottom holes (FBHs) or side-drilled holes (SDHs). These blocks are often used to determine system sensitivity and to perform distance-amplitude correction (DAC) curves. However, the construction of DAC curves in this manner is expensive and not always a simple procedure since a large number of specimens with appropriate curvatures and reference reflectors located at different depths in the specimen are needed. Therefore, less costly and quantitative methods are strongly needed. To address such a need, theoretical ultrasonic models can be a very promising tool.

To date, extensive research has been carried out to develop theoretical ultrasonic beam and flaw scattering models. As a result, there now are available very versatile ultrasonic measurement models that allow one to simulate the signals measured in many ultrasonic setups (Thompson and Gray, 1983, Sedov et al, 1992, Schmerr, 1998). As an example of using such ultrasonic measurement models, Schmerr and Thompson (Schmerr and Thompson, 1997) reported on the pioneering work of T. Gray at the Center for NDE, Iowa State University, who showed that one can simulate the DAC curves for FBHs located beneath planar, convex, and concave surfaces and proposed model-based curvature correction factors to compensate for curvature effects and relate the measurements on curved specimens to those on less costly planar specimens.

In this study, we will show that a model-based approach similar to that described by

Received: October 9, 2003. Accepted: November 20, 2003. * Center for NDE, Iowa State University, Ames, IA, 50011 USA, ** Dept. of Aerospace Eng., Iowa State University, Ames, IA, 50011 USA, *** School of Mechanical Eng., Sungkyunkwan University, Suwon 440-746 Korea, **** Dept. of Mechanical Eng., Lakehead University, Thunder Bay, Ontario, P7B 5E1 Canada, † Corresponding author: hjkim21c@cnde.iastate.edu

Schmerr and Thompson can be used in a much more general context. Specifically, we will show that one can obtain model-based transfer curves that allow one to account for different calibration block surface curvatures, flaw type (SDH or FBH), and flaw size and thus relate the DAC curve for one setup configuration to another quite different configuration. This transferring of DAC curves from one case to another will be demonstrated with a specific example.

2. Ultrasonic Measurement Models

To construct DAC curves for a FBH or a SDH theoretically, we need to have an ultrasonic measurement model for the test set-ups shown in Fig. 1 where the scatterer is either a FBH or a SDH. Below, we will present suitable measurement models for both of these reflectors.

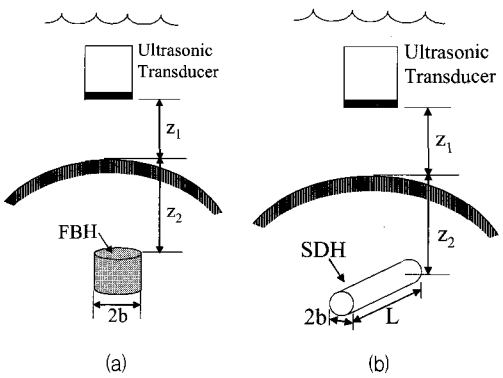

Fig. 1 Schematic diagrams of the pulse-echo immersion testing for (a) a FBH and (b) a SDH in the solid specimen

2.1. Ultrasonic measurement models

All of the measurement models used in this study are based on a reciprocity-based relationship, similar to that originally derived by Auld (Auld, 1979), where the frequency components of the received voltage, $V_R(\omega)$, (for harmonic disturbances of the form $\exp(-i\omega t)$), are related to stress and velocity fields on the surface of the scatterer in two problems, labeled a and b, respectively. The fields in problem a are due to the transducer firing with the scatterer present while in problem b the fields are with the scatterer absent. The frequency component of the received voltage $V_R(\omega)$ in terms of these fields can be expressed as (Schmerr, 1998)

$$V_R(\omega)=\frac{\beta(\omega)}{2\rho_1 c_1^p v_0^{(a)} v_0^{(b)} S_T}\int_{S_f}\left(\tau_{ij}^{(a)}v_j^{(b)}-\tau_{ij}^{(b)}v_j^{(a)}\right)n_i dS \tag{1}$$

where $(\tau_{ij}^{(m)}, v_j^{(m)})$ are the stresses and velocity fields for problems $m=a, b$, respectively, S_T is the area of the transducer and S_f is the surface of the scatterer, n_i are components of the outward normal to the scatterer (pointing into the solid), ρ_1, c_1^p are the density and wave speed of the fluid, and $v_0^{(m)}$ are the velocities on the face of the transducer, which we consider as a piston source, for problems $m=a, b$. The quantity $\beta(\omega)$ is the system efficiency factor, which can be obtained through the measured voltage in a particular reference calibration setup (Schmerr et al, 1994).

In applying Eq. (1), we will make several assumptions that will greatly facilitate the modeling of the reference scatterer. First, we will assume that the transducer wave field incident on the scatterer in problem a and b can be written in a quasi-plane wave form (paraxial approximation) (Schmerr, 1998). For the fields in the problem b, for example, we have $v^{(b)}=\hat{V}^{\alpha}(\omega)v_0^{(b)}\mathbf{d}^{\alpha}\exp\left(ik_2^{\alpha}\mathbf{e}^{\alpha}\cdot\mathbf{x}\right)$ where $\hat{V}^{\alpha}(\omega)$ is a normalized velocity amplitude (that depends upon $\boldsymbol{x}$ as well as ω, but only the ω dependency is shown for simplicity), and $\mathbf{e}^{\alpha}$, $\mathbf{d}^{\alpha}$ are unit vectors describing the incident wave direction and polarization, respectively, for a wave of type α ($\alpha=p, sv$) and $k_2^{\alpha}=\omega/c_2^{\alpha}$ is the corresponding wave number. With this assumption Eq. (1) becomes

$$V_R(\omega)=\beta(\omega)\left[\frac{2}{-ik_2^{\alpha}r^2}\frac{\rho_2 c_2^{\alpha}}{\rho_1 c_1^{p}}\right]\int_{S_f}\left(\hat{V}^{\alpha}(\omega)\right)^2 G^{\alpha}\exp\left(ik_2^{\alpha}\mathbf{e}^{\alpha}\cdot\mathbf{x}\right)dS(\mathbf{x}) \tag{2}$$

where r is the radius of the transducer, ρ_2 is the density of the solid, and c_2^{α} ($\alpha = p, sv$) are the wave speeds of compressional and shear waves in the solid. The quantity G^{α} is given by

$$G^{\alpha}=\frac{1}{4\pi\rho_2\left(c_2^{\alpha}\right)^2}\left[\tilde{\tau}_{ij}^{\alpha}n_i d_j^{\alpha}+d_k^{\alpha}e_l^{\alpha}\frac{C_{ijkl}n_i\tilde{v}_j^{\alpha}}{c_2^{\alpha}}\right] \tag{3}$$

where $\tilde{\tau}_{ij}^{\alpha},\tilde{v}_j^{\alpha}$ are the stresses and velocity components on the surface of the scatterer due to an incident plane wave of type α ($\alpha = p, sv$) and unit displacement amplitude.

2.2. Measurement model for a FBH

For a small FBH where the beam variations over the flaw surface are negligible, the velocity amplitude term, $\left(\hat{V}^{\alpha}\right)^2$ over the surface of the scatterer can be removed from the integral. The integral of G^{α} over the surface of the scatterer then corresponds to the far-field scattering amplitude of the scatterer. Therefore, the received voltage from a FBH can be written as

$$V_{FBH}(\omega)=\beta(\omega)\left[\hat{V}^{p}(\omega)\right]^2 A_F(\omega)\left[\frac{c_2^{p}}{-i\pi f r^2}\frac{\rho_2 c_2^{p}}{\rho_1 c_1^{p}}\right] \tag{4}$$

where f is the frequency and $\hat{V}^{p}(\omega)$ is the normalized velocity amplitude which is calculated using a beam model such as a multi-Gaussian beam model (Schmerr, 2000). For such a beam model we have

$$\hat{V}^{p}(\omega)=\sum_{n=1}^{N}\mathbf{d}^{\alpha}\frac{A_n}{1+\left(\frac{iB_n D_f}{x_r}\right)}T_{12}^{p,p}\frac{\sqrt{\det\mathbf{G}_2^{p}(0)}}{\sqrt{\det\mathbf{G}_2^{p}(z_2)}}\exp(ik_1 z_1)\exp(ik_2^{p}z_2)\exp\left[\frac{ik_1\mathbf{x}^T\left[\mathbf{G}_2^{p}(z_2)\right]^{-1}\mathbf{x}}{2}\right] \tag{5}$$

where, A_n, B_n are height and width factors of individual Gaussian beams, z_1 is the distance from transducer to interface, z_2 is the distance from interface to the flaw, $x_r=(1/2)k_1 r^2$ is the Rayleigh distance, $T_{12}^{p,p}$ is the transmission coefficient, and $\mathbf{G}_2^{p}(0)$, $\mathbf{G}_2^{p}(z_2)$ matrices were defined in detail by Schmerr (Schmerr, 2000).

Based on the Kirchhoff approximation, the pulse-echo far-field scattering amplitude from a FBH at normal incidence, $A_F(\omega)$, can be written as (Schmerr and Sedov, 2003):

$$A_F(\omega)=\frac{ik_2^{p}b^2}{2} \tag{6}$$

where $k_2^{p}=\omega/c_2^{p}$ is the wave number in the solid, and b is the radius of the FBH.

For a large FBH where beam variations are important, Eq. (4) can still be used, but where the FBH surface is broken into rings and the total response calculated as the sum of the response of each of those rings (Schmerr and Sedov, 2003).

2.3. Measurement model for a SDH

For modeling the response of a SDH, Eq. (4) is not suitable since the incident fields can extend a significant distance along the length of the hole. However, if one assumes that the scattered wave field of the SDH can be obtained from the Kirchhoff approximation (Schmerr, 1998) then Eq. (2) reduces to

$$V_R(\omega)=\beta(\omega)\left[\frac{i}{\pi r^2}\frac{\rho_2 c_2^{\alpha}}{\rho_1 c_1^{p}}\right]\int_{C_{lit}}\left(\mathbf{e}^{\alpha}\cdot\mathbf{n}\right)\exp\left(2ik_2^{\alpha}\mathbf{e}^{\alpha}\cdot\mathbf{x}\right)\left[\int_L\left(\hat{V}^{\alpha}(\omega)\right)^2 dy\right]dC(\mathbf{x}) \tag{7}$$

where C_{lit} is a line integral over the lit portion of the cylinder surface, and L is the length of the SDH, which is taken larger than the length over which beam variations are important.

If the beam variations over the cross-section of a SDH are negligible, the received voltage from a SDH can be calculated by (Schmerr and Sedov, 2003),

$$V_{SDH}(\omega)=\beta(\omega)\frac{1}{L}\left[\int_L\left(\hat{V}^{p}(\omega)\right)^2 dy\right]A_S(\omega)\left[\frac{c_2^{p}}{-i\pi f r^2}\frac{\rho_2 c_2^{p}}{\rho_1 c_1^{p}}\right] \tag{8}$$

The corresponding pulse-echo far-field scattering amplitude at normal incidence from a SDH of radius b and length L, obtained by using Kirchhoff approximation, can be written as

$$A_S(\omega)=L\frac{-ik_2^p b}{2}\left\{S_1\left(2k_2^p b\right)+iJ_1\left(2k_2^p b\right)-\frac{2}{\pi}\right\} \quad (9)$$

where S_1 and J_1 are Struve and Bessel functions, respectively.

Model studies have shown that a more general SDH model which takes into account beam variations gives essentially the same results as the above model (Schmerr and Sedov, 2003). Thus, here we have based all of our SDH modeling results only on Eq. (8).

2.4. System Efficiency Factor

The system efficiency factor, $\beta(\omega)$, can be computed by the deconvolution of an experimental signal obtained from a reference reflector by a corresponding theoretical reference reflector model, as given in Eq. (10) (Schmerr et al, 1994):

$$\beta(\omega)=\frac{V_r(\omega)}{<v_m(\omega)>/v_0}W(\omega) \quad (10)$$

where $V_r(\omega)$ is an experimentally measured voltage, $\langle v_m(\omega)/v_0\rangle$ is the average received velocity by the theoretical reference model and $W(\omega)$ is a Wiener filter.

If we take the plane interface (the front surface of a specimen immersed in water) to be our reference reflector in our immersion testing setup, then $\langle v_m(\omega)/v_0\rangle$ is given by (Rogers and Van Buren, 1974):

$$<v_m(\omega)>/v_0=R_{12}^{p,p}\exp(2ik_1z_1)\left\{1-\exp\left(\frac{ik_1r^2}{2z_1}\right)\left[J_0\left(\frac{k_1r^2}{2z_1}\right)-iJ_1\left(\frac{k_1r^2}{2z_1}\right)\right]\right\} \quad (11)$$

where $R_{12}^{p,p}$ is the reflection coefficient of a plane compressional wave for a planar fluid-solid interface, and J_0 and J_1 are the Bessel functions of the zero and first order, respectively.

2.5. Model Verification

In order to gain confidence in using model-based DAC curves, we need to verify that the measurement models do indeed work for these setups. To show this, both measurement models were compared to the experimental signals measured from two different flaw sizes: 1.19 mm (3/64 inch) and 3.18 mm (8/64 inch) diameter FBHs, and 1 mm (2.56/64 inch) and 4 mm (10.24/64 inch) diameter SDHs which are the smallest and the largest flaw considered in this study. To determine the system efficiency factor of

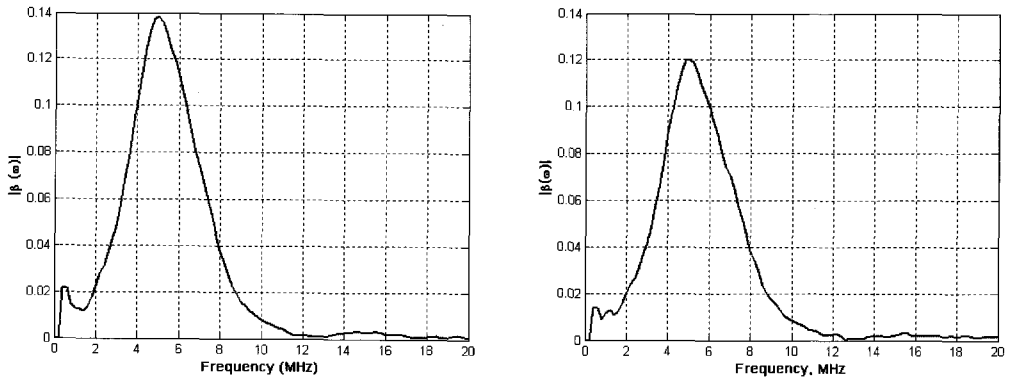

(a) (b)

Fig. 2 System efficiency factor measured for the planar transducer of 5 MHz center frequency, 1/4 inch diameter from (a) the ASTM resolution block and (b) aluminum block with a 2 inch water path

these ultrasonic measurement systems, the front surface reflection signals were captured from an ASTM resolution block (which contains 1.19 (3/64), 1.98 (5/64) and 3.18 mm (8/64 inch) diameter FBHs located at from 0.05 inch to 1.25 inch metal paths) and an aluminum specimen (which contains 1 mm (2.65/64 inch) and 4 mm (10.24/64 inch) diameter SDHs at a 25.4 mm metal path) immersed in water. The transducer used was a 5MHz center frequency planar transducer 3.65 mm in diameter and the water path length from transducer to block was 50.8 mm water path. By deconvolution of these signals by the reference reflector model (Eq. 11) we determined the system efficiency factors of these measurement systems as shown in Fig. 2 (a) and (b).

Fig. 3 and Fig. 4 show the comparison between experimentally measured signals and predicted time domain waveforms for the FBHs and SDHs, respectively. As shown in Fig. 3 and Fig. 4, the agreement between the theoretical prediction and the experiments is very good, demonstrating the validity of the models in these cases.

3. Model-based DAC curves

As mentioned before, to construct model-based DAC curves for reference reflectors (FBHs and SDHs), the system efficiency factor

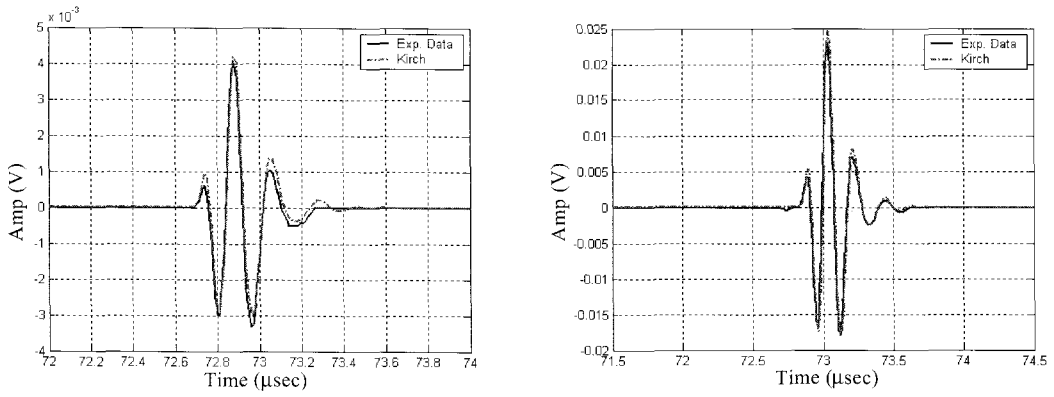

Fig. 3 Comparison of predicted flaw signals from (a) a 3/64 inch diameter FBH and (b) an 8/64 inch diameter FBH with experiments. Solid line: measured signal, dotted line: predicted signal.

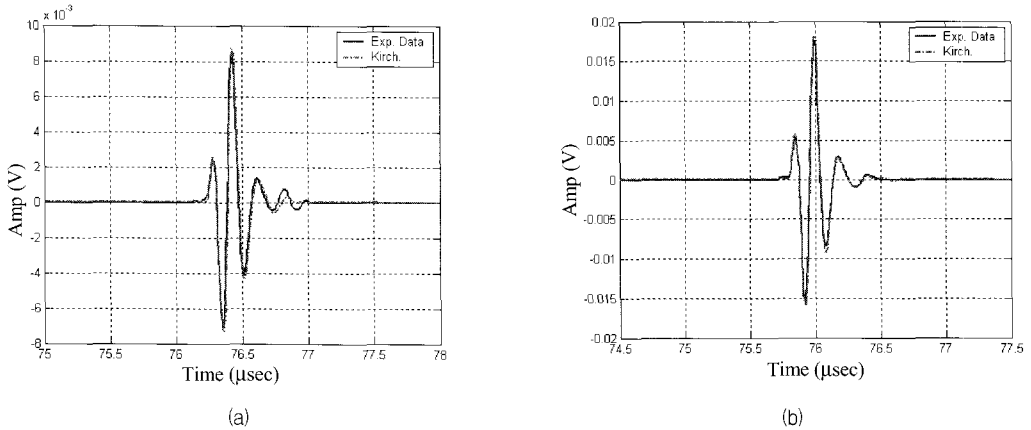

Fig. 4 Comparison of predicted flaw signals from (a) a 1 mm diameter SDH and (b) a 4 mm diameter SDH with experiments. Solid line: measured signal by experiment, dotted line: predicted signal.

needs to be known. In this study, in order to specify a system efficiency factor, the measured voltage in the time domain, $V_0(t)$, for the reflection from a plane surface is assumed to be given by Eq. (12) which was also used in the benchmark study (Thompson, 2002 and Schmerr, 2002).

$$V_0(t)=\begin{cases}\left[1-\cos\left(\dfrac{2\pi f_c}{2}t\right)\right] & for \quad 0\le t\le \dfrac{3.0}{f_c}\\ 0 & otherwise\end{cases} \tag{12}$$

where t is the time in microseconds and f_c is the center frequency of the transducer, in MHz. Fig. 5 (a) and (b) show the calculated reference signal by use of Eq. (12) and the system efficiency factor (obtained by using Eq. (11) and Eq. (12)) for a planar transducer of 5MHz center frequency, 6.35 mm diameter.

Using the ultrasonic measurement models previously described (Eq. (4) and Eq. (8)) and the system efficiency factor, we obtained the complete A-scan waveforms from which we calculated the peak-to-peak voltages. By varying the metal path length and plotting these peak-to-peak voltages we constructed DAC curves for FBHs and SDHs for different flaw sizes and interface curvatures. In all cases, the water path distance remained fixed at a distance of 50.8 mm.

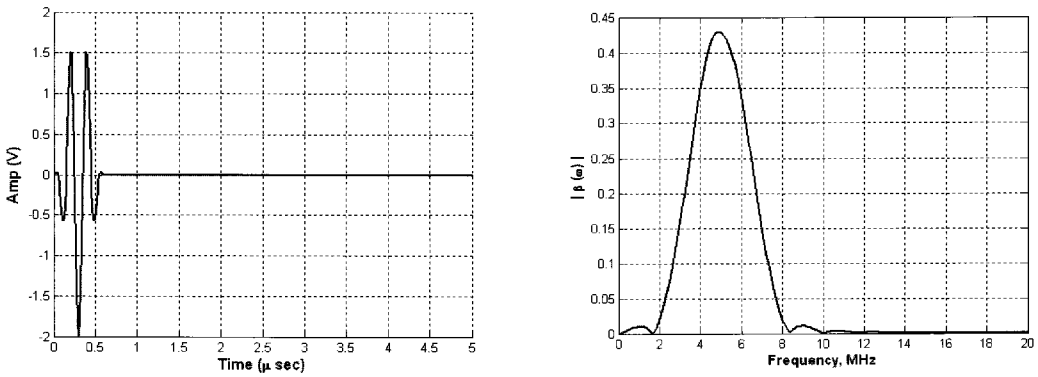

(a) (b)

Fig. 5 (a) The reference reflection signal using Eq. (12), and (b) the system efficiency factor for the planar transducer: 5 MHz center frequency, 0.5 inch diameter

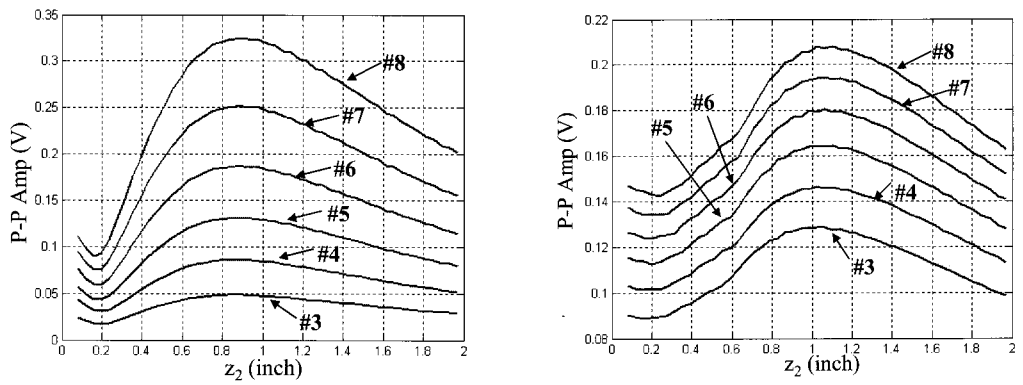

(a) (b)

Fig. 6 Model-based DAC curves for (a) FBHs, (b) SDHs in an aluminum specimen with planar interface immersed in the water with variation in the metal distance (from 2 mm (0.07 inch) to 50.8 mm (2 inch)).

In the case of flaw size, we chose six different diameters of flaws ranging from 1.19 mm (3/64 inch, designate by #3) to 3.18 mm (8/64 inch, designate by #8) in steps of 1/64 inch. And, we considered two types of interface curvatures: convex and concave with a variation of the radius of curvature from 76.2 mm (3 inch) to 203.2 mm (8 inch) in steps of 25.4 mm (1 inch). In this paper, we only show the predicted DAC curves for FBHs and SDHs in a planar, 101.6 mm (4 inch) radius (convex), and -101.6 mm (-4 inch) radius (concave) aluminum specimen at different depths from the surface. Figs. 6 through 8 show the constructed model-based DAC curves for FBHs and SHDs using our ultrasonic measurement models.

4. Transferring DAC curves

4.1. Transfer curves

Based on model-based DAC curves, we propose three types of new transfer curves: interface transfer curves, flaw type transfer curves, and flaw size transfer curves.

To obtain the interface transfer curves, we calculated the amplitude ratio between the planar interface DAC curves and the convex and concave interface DAC curves for both the FBH and SDH. In Fig. 9 are shown the transfer curves from planar to convex interface obtained from taking the ratio of the values of DAC curves for convex interface to the DAC curves for the

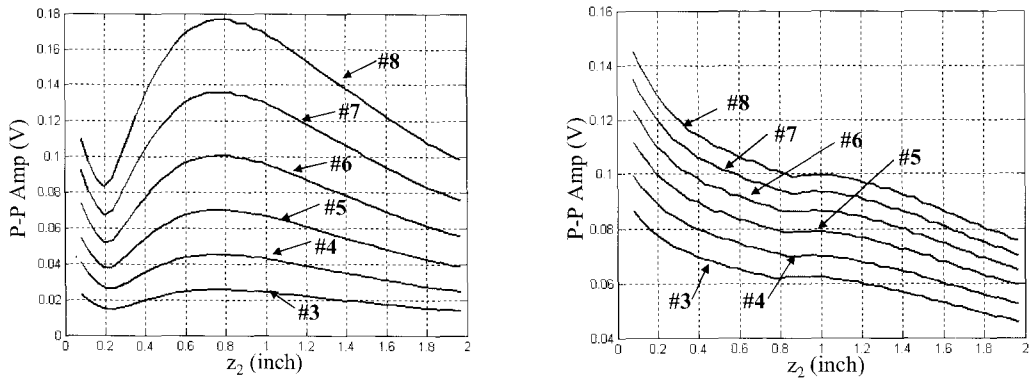

Fig. 7 Model-based DAC curves for (a) FBHs, (b) SDHs in an aluminum specimen with 4 inch radius convex interface immersed in the water with variation in the metal distance (from 2 mm (0.07 inch) to 50.8 mm (2 inch)).

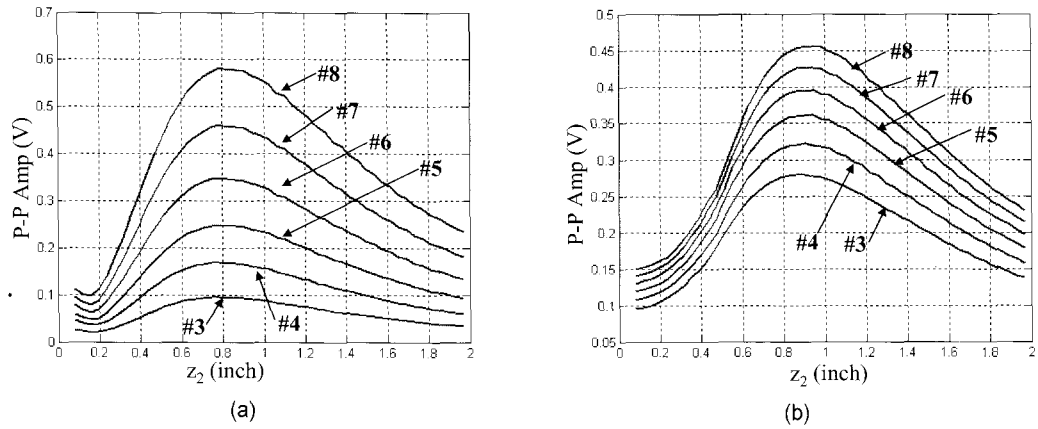

Fig. 8 Model-based DAC curves for (a) FBHs, (b) SDHs in an aluminum specimen with -4 inch radius concave interface immersed in the water with variation in the metal distance (from 2 mm (0.07 inch) to 50.8 mm (2 inch)).

planar interface. And in Fig. 10 are shown the interface transfer curves from planar to concave interface obtained through ratio of the values of DAC curves for concave interface to DAC curves for the planar interface. In both cases, the interface transfer curves strongly depend on the flaw type and radius of curvature of the interface but depend only very weakly on the flaw size. Thus, these curves can compensate for the interface curvature effect and allow us to construct DAC curves for either a convex and concave interface from already measured DAC curves from a planar interface, which are always simpler (and cheaper) to obtain.

To obtain transfer curves for flaw type, we calculate amplitude ratio between the DAC curves for a FBH and SDH based on our model-based curves. Fig. 11 shows the flaw type transfer curves from SDH to FBH in a planar interface specimen obtained from taking the ratio of the values of DAC curves for the SDH to DAC curves for the FBH. However, these flaw type transfer curves do not depend on the radius of curvature of the interface. Therefore, we can use the flaw type transfer curves for a planar interface only to account for change in the flaw type.

To account for flaw size, we construct the flaw size transfer curves by calculating the amplitude ratio of a set of DAC curves for six different size flaws to the amplitude of the DAC curves corresponding to the #5 flaw size. Fig. 12 shows the flaw size transfer curves. Also, these curves do not depend on the interface radius of curvature.

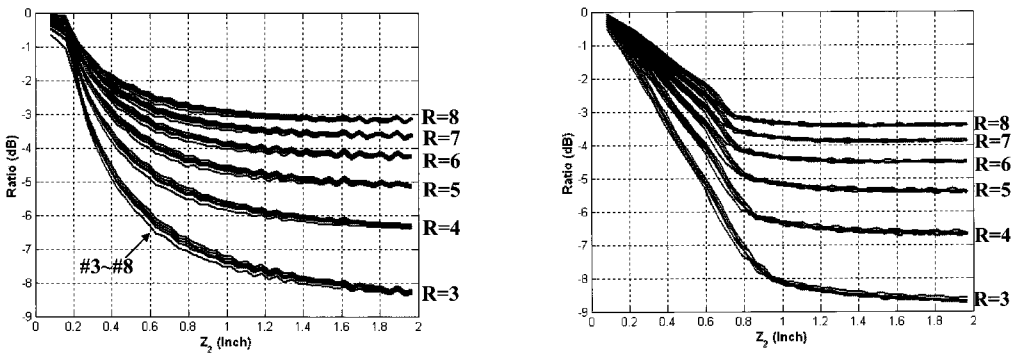

Fig. 9 Interface transfer curves for (a) FBHs and (b) SDH from planar interface to convex interface (ratio of values of DAC curves for the convex interface to the planar interface)..

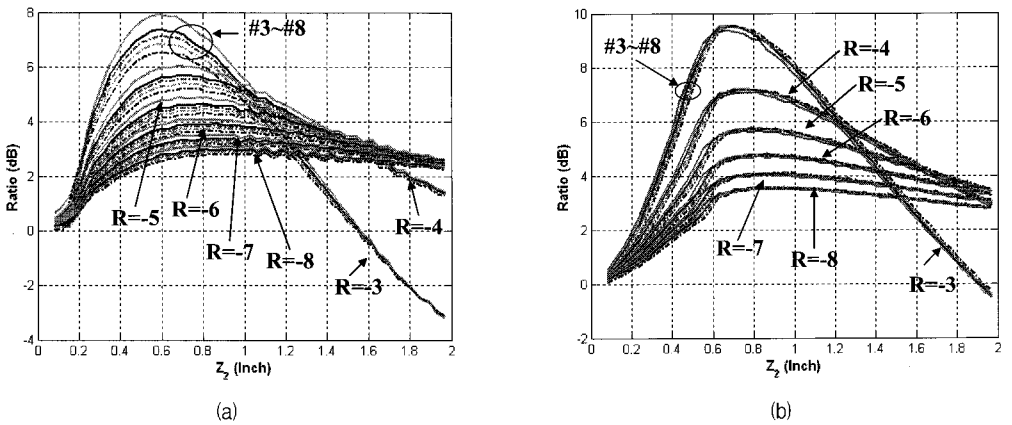

Fig. 10 Interface transfer curves for (a) FBHs and (b) SDHs from planar interface to concave interface (ratio of the values of concave interface DAC curves to the planar interface DAC curves).

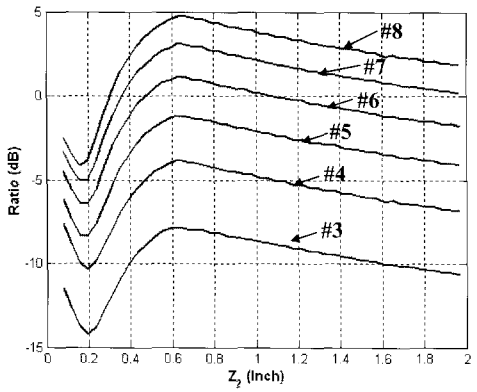

Fig. 11 The flaw type transfer curves from SDH to FBH (ratio of values of DAC curves for the SDH to the FBH for the planar interface)

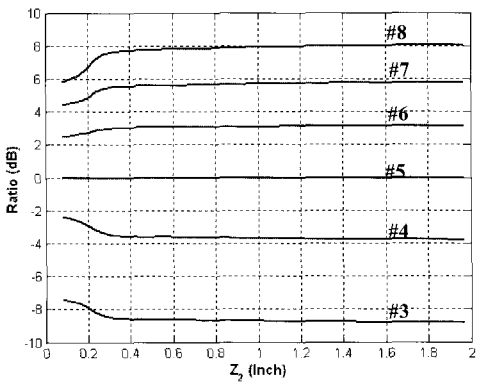

Fig. 12 The flaw size transfer curves for size difference (ratio of #3 ~ #8 DAC curves to #5 DAC curves for the planar interface)

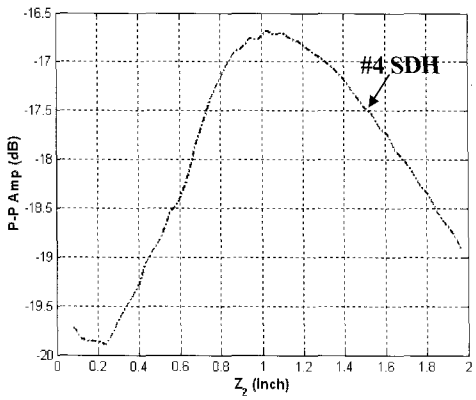

(a)

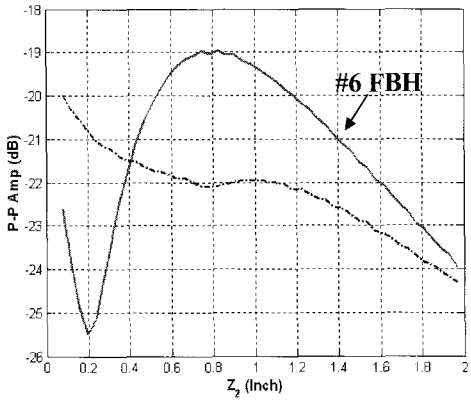

(b)

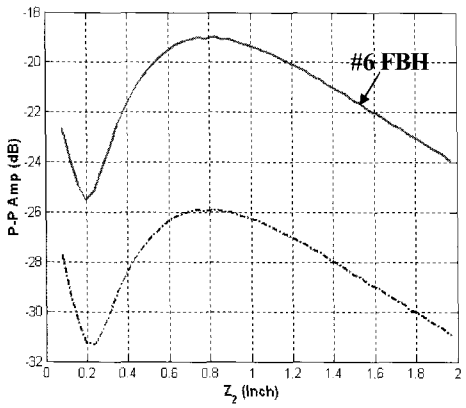

(c)

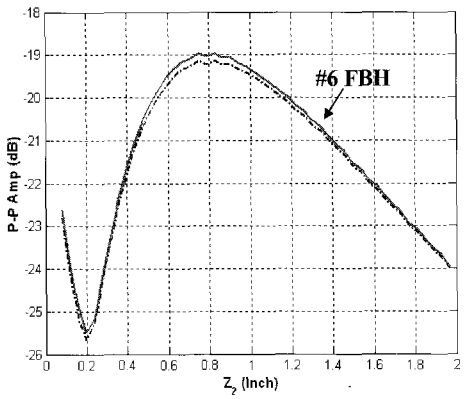

(d)

Fig. 13 Example of transferring DAC curves from DAC curves for #4 SDH with planar interface to DAC curves for #6 FBH with convex interface. (a) DAC curves for #4 SDH with planar interface, (b) after using curvature transfer curves, (c) after using flaw type transfer curves, and (d) after using flaw size transfer curves. Solid line: desired DAC curve, dotted one: transferred DAC curve.

4.2. Example

To demonstrate the use of the proposed transfer curves, we propose to start with the DAC curve for a #4 SDH in a planar interface specimen and show how the transfer curves can transform this starting DAC curve into a "desired" DAC curve for a #6 FBH in a 5 inch radius convex interface specimen. Fig. 13 (a) shows the model based DAC curve for the #4 SDH in the planar interface specimen. In order to obtain the DAC curve that will correspond to the #6 FBH in the convex interface specimen, we first multiply the starting DAC curve by the appropriate interface transfer curve (Fig. 9 (b), R = 5) to account for the change in interface curvature. Fig. 13 (b) shows the transferred DAC curves after using the interface transfer curves along with our final goal, i.e. the desired DAC curve which is the DAC curve for a #6 FBH in a convex interface specimen. Second, we apply the flaw type transfer curves (Fig. 11, #4) to account for the change in flaw type to obtain the DAC curve for a #4 FBH beneath a 5 inch radius convex interface, as shown in Fig. 13 (c) (where again we show the final desired DAC curve). Finally, we use the flaw size transfer curve (Fig. 12, #6) to go from a #4 FBH to a #6 FBH. In Fig. 13 (d) we compare the desired DAC curves for #6 FBH to the transferred DAC curve obtained from DAC curves for #4 SDH shown in Fig. 13 (a). As shown in Fig. 13 (d), the accuracy obtained using the proposed transfer curves is indeed excellent (less than 0.3 dB).

Conclusions

In this study, we proposed a new and efficient approach to obtain DAC curves using an ultrasonic measurement model. We constructed DAC curves theoretically for both a flat-bottom hole (FBH) and a side-drilled hole (SDH) for different flaw sizes and interface curvatures. Based on these model-based DAC curves, we proposed three types of transfer curves that account for interface curvature, flaw type, and flaw size. In addition, we demonstrated the use of these transfer curves to "morph" the DAC curve for a SDH in a planar specimen to the DAC curve for a FBH of different size in a curved specimen. If these procedures are carefully validated experimentally, they can form the basis for a new set of highly efficient and cost-effective tools for ultrasonic systems.

Acknowledgements

L. W. Schmerr and Hak-Joon Kim were supported in this work by the Center for NDE, Iowa State University through the National Science Foundation Industry / University Cooperative Research Center Program. A. Sedov would like to acknowledge support by the Natural Sciences and Engineering Research Council of Canada.

References

Thompson, R. B. and Gray, T. A. (1983) A model relating ultrasonic scattering measurements through liquid-solid interfaces to unbounded medium scattering amplitudes, Journal of Acoustical Society of America, Vol. 74, pp. 1279-1290

Sedov, A., Schmerr, L. W., and Song S. J (1992) Ultrasonic Scattering by a Flat-bottom Hole in Immersion Testing: An Analytical model, Journal of Acoustical Society of America, Vol. 92, pp. 478-486

Schmerr, L. W. (1998) Fundamentals of Ultrasonic Nondestructive Evaluation - A Modeling Approach, Plenum Press, New York

Schmerr, L. W. and Thompson, D. O. (1997) The Role of Modeling in NDE standards,

European-American Workshop, Determination of Reliability and Validation of NDE, Germany, pp. 321-328

Auld, B. A (1979) General Electromechanical Reciprocity Relations Applied to the Calculations of Elastic Wave Scattering Coefficients, Wave Motion, Vol. 1, pp. 3-10

Schmerr, L. W and Sedov, A. (2003) Modeling ultrasonic problems for the 2002 Benchmark session, in Review of Progress in Quantitative Nondestructive Evaluation, Vol. 22, eds. D. O. Thompson and D. E. Chimenti, AIP, New York, pp. 1776-1783

Schmerr, L. W. (2000) A Multi-Gaussian Ultrasonic Beam Model for High Performance Simulations on a Personal Computer, Materials Evaluations, Vol (58), pp.882-888

Schmerr, L. W., Song J. S. and Zhang. H. (1994) Model-Based Calibration of Ultrasonic System Responses for Quantitative Measurements, Nondestructive Characterization of Materials VI, pp. 111-118

Rogers, P. H and Van Buren, A. l. (1974) An Exact Expression for the Lommel Diffraction Correction Integral, Journal of Acoustical Society of America, Vol. 55, pp. 724-728

Thompson, R. B. (2002) An Ultrasonic Benchmark Problem: Overview and Discussion of Results, in Review of Progress in Quantitative Nondestructive Evaluation, Vol. 21, eds. D. O. Thompson and D. E. Chimenti, AIP, New York, pp. 1917-1924

Schmerr, L. W. (2002) Ultrasonic Modeling of Benchmark Problems, in Review of Progress in Quantitative Nondestructive Evaluation, Vol. 21, eds. D. O. Thompson and D. E. Chimenti, AIP, New York, pp. 1933-1940